Hindawi
Shock and Vibration
Volume 2021, Article ID 8871458, 14 pages
https://doi.org/10.1155/2021/8871458

Research Article

Experimental Investigation on the Mechanical Response of Coals to Uniaxial Compression and Low-Speed Dynamic Loading

Jing-Xuan Zhou[1], **Chuan-Jie Zhu**[1], **Xi-Miao Lu**[1], **Jie Ren**[1], **Rong-Jun Si**[2] and **Qing Ye**[3]

[1]*Faculty of Safety Engineering, China University of Mining and Technology, Xuzhou, Jiangsu 221116, China*
[2]*China Coal Technology Engineering Group Chongqing Research Institute, Chongqing 400039, China*
[3]*School of Resource & Environment and Safety Engineering, Hunan University of Science and Technology, Xiangtan, Hunan 411201, China*

Correspondence should be addressed to Chuan-Jie Zhu; anq021@126.com

Received 24 March 2020; Revised 17 December 2020; Accepted 21 December 2020; Published 6 January 2021

Academic Editor: Roman Gabl

The surrounding rock of roadways in underground coal mines will lose its stability or even collapse under gas explosions, especially roadways surrounded by coals. The dynamic mechanical properties of coals were tested in order to investigate the dynamic response of coals under gas explosions. The static mechanical properties of coals were also tested as comparison. It is found that the dynamic stress-strain curves showed no obvious pore compaction stage comparing with uniaxial loading. The dynamic compression strength and the elastic modulus are obviously larger than those obtained in the static mechanical properties test, and the dynamic strain shows an obvious hysteresis phenomenon. The ultimate strain and absorbed energy increased linearly with increase of the strain rate. With the increase of dynamic loading, the fragment size of coal cores decreased obviously. The results could provide a reference for the antiexplosion design of the coal roadway.

1. Introduction

Gas explosion (premixed methane-air explosions) occurring in underground coal mines is a great threat to the coal mining industry, which leads to large amounts of deaths and economic losses. Moreover, the blast wave of gas explosions can also destroy the surrounding rock (mainly refers to coal) of roadways [1–3], which causes failure or collapse of roadways. As a result, the escaping route will be blocked, which makes the miners be trapped. The theoretical detonation pressure of gas explosions is as low as 1.76 MPa and about 4 MPa due to reflection [4], which is much lower than the strength of TNT explosions. However, there are no obtained results explaining why the roadway collapses under such low pressure and how to prevent that. Therefore, understanding the static and dynamic mechanical properties of coal can provide a basic means to evaluate the stability of coal mine roadways under quasistatic ground stress and dynamic explosion loading.

There are two main methods for evaluating the strength of coal and rock: one is the commonly used static loading test [5] and the other is the dynamic loading test. In fact, during the gas explosions, both the static loading and dynamic loading play an important role in the damage of coal and rock. Static loading (mainly refers to ground stress) causes prestress damage to the surrounding rock of the roadway [6, 7] and thus reducing its strength, which makes the surrounding rock more susceptible to lose stability under gas explosions [8–10]. The dynamic loading (mainly refers to the blast wave of gas explosions) with a very sharp loading rate may destroy the roadways at a lower pressure. In addition, gas explosions usually occur in the working face or the heading face. The type of surrounding rock of roadways is mainly coal with a lower strength, and the dynamic fracture of the coal is more obvious than other damage. Besides, coal is a type of highly heterogeneous material [11–13]. Many previous studies have shown that the failure mode of coal is characterized by the development of internal fractures under

loading and ultimately leading to macroscopic damage [14–16]. For the static loading method, the uniaxial compression test is mainly used to study the static mechanical properties [17]. The dynamic loading of the explosion will affect the stability of the surrounding rock. The commonly used dynamic loading technique is the Hopkinson bar experiment [18–21].

Recently, many scholars have done research studies on the static and dynamic mechanical properties of rocks and coals by both experiment and numerical simulation [22–27]. Yilmaz and Unlu [28] used three-dimensional numerical simulation to study the dynamic and static strength and strain of rock. Zhang et al. [29] investigated the failure characteristics of materials under the coupling of static stress and explosion loading. Previous researchers have carried out a lot of work on coal and rock static and dynamic experiments focusing on the dynamic stress and strain, energy dissipation, and fragmentation. Zhu et al. [30] conducted a dynamic and static mechanical performance test on a rock with a high strength load of 80 MPa based on the modified separate Hopkinson pressure bar (SHPB) test system. The results show that the change of stress value can significantly change the failure mode of the rock surface regardless of the application of static stress or biaxial stress. Huang and Subhash [31] established a dynamic damage growth model of rocks under biaxial compression loading.

Most of the previous research studies have studied the static and dynamic mechanical characteristics of rocks with high strength; meanwhile, many research studies have studied the high dynamic loading of coals (a kind of porous rock with very low strength). The dynamic mechanical properties of coal under low-speed loading are rarely studied. In the present work, the dynamic response of coals to low-speed dynamic loadings (equivalent to three different overpressure levels of gas explosions) was studied. The static mechanical properties were also studied as a comparison.

2. Experiments

2.1. Sample Preparation. Two kinds of coals with different strength were selected in our experiments, e.g., anthracite coal and bituminous coal. They were taken from Jiaozuo Coal Mine and Xinbei Coal Mine, China, respectively. Proximate analysis results of them are given in Table 1. Cylindrical coal cores were used in our tests and were cut from large coal blocks. The diameter of the coal cores used in the static mechanical properties test was 50 mm with a height of 100 mm. It was 100 mm and 50 mm, respectively, in the dynamic mechanical properties test. Figure 1 shows photos of the coal cores used in our experiments. The differences between static mechanical test and dynamic mechanical test are crucial. As for the uniaxial compression test, its standard sample size is 50 mm in diameter and 100 mm in height. For the SHPB test, we would minimize axial and radial inertia effects to improve the reliability of experimental results [18, 32], so we have decreased the height diameter ratio and selected the coal specimens 100 mm, and the height is 50 mm.

2.2. Experimental System

2.2.1. Static Mechanical Properties Test System. The static stress-strain curve, mechanic parameters, and acoustic emission characteristics of the coal cores were tested by a uniaxial compression experiment system (shown in Figure 2). Compared with triaxial compression tests, the uniaxial compression test has limitation, but it can directly reflect the most basic mechanical properties of coal, which is the most basic reference standard [5]. The system mainly includes a compression loading system (MTS C64.605, MTS Industrial System CO.LTD), a stress-strain acquisition system, an acoustic emission system, and other accessories. The loading rate of the MTS system is 0.1 mm/min in our experiments. The stress-strain evolution of the coal cores is monitored by the stress-strain acquisition system (DH3817, Tonghua Testing Technology Co. LTD, China). Meanwhile, the acoustic emission (AE) acquisition system (DS5, Beijing Softland Times Scientific & Technology Co. LTD, China) is used to monitor the AE signal.

2.2.2. Dynamic Mechanical Properties Test System. The SHPB (split Hopkinson pressure bar) is used to study the dynamic mechanical properties of coals, a schematic diagram of which is shown in Figure 3. The SHPB includes a pressure bar system (including a high pressure nitrogen bottle, an air chamber, a launch cavity, a striker bar, an incident bar, a transmission bar, and an adsorption bar), air pressure controller, speed measuring system (including speed measuring circuit and time interval instrument), strain collection system (including two strain gauges and transient waveform storage instrument), and data processing system. The diameter of bars is 100 mm. The length of the striker bar and the transmission bar with an elastic modulus of 210 GPa is 2 m.

During the tests, the striker bar impacts the free end of the incident bar and produces longitudinal compression wave (incident wave) in the incident rod. When the compression wave arrives at the interface between the incident bar and coal core, it is partly reflected (reflected wave) and the rest passes through the coal core into the transmission bar (transmitted wave). Based on the assumption of one-dimensional stress wave and stress homogenization [33], the dynamic response parameters of the coal cores can be calculated by following formulas [18]:

$$\dot{\varepsilon} = \frac{C_0}{l_0}\left(\varepsilon_i - \varepsilon_r - \varepsilon_t\right), \tag{1}$$

$$\varepsilon = \frac{C_0}{l_0}\int_0^t \left(\varepsilon_i - \varepsilon_r - \varepsilon_t\right)\mathrm{d}t, \tag{2}$$

$$\sigma = \frac{A}{2A_0}E\left(\varepsilon_i + \varepsilon_r + \varepsilon_t\right), \tag{3}$$

where, $\dot{\varepsilon}$, ε, and σ are the strain rate, strain, and stress of the coal cores; ε_i, ε_r, and ε_t are the incident, reflected, and transmitted strain, respectively; C_0, l_0, and E are the wave

Table 1: Proximate analysis results of the coal cores.

Materials	Moisture (%)	Ash (%)	Volatile (%)	Carbon (%)	R_0 (%)
Anthracite coal	2.49	8.78	8.63	83.35	3.09
Bituminous coal	9.07	11.34	34.02	57.75	0.58

(a) (b)

Figure 1: Photos of coal cores used in the experiments. (a) Cores used in the test of static mechanical properties and (b) cores used in the test of dynamic mechanical properties.

velocity of elastic wave, length of the coal core, and elastic modulus of the bar, respectively; and A and A_0 are the cross-section area of the bar and coal cores, respectively.

According to the assumption of stress homogenization of coal cores, it can also be obtained that

$$\varepsilon_t = \varepsilon_i + \varepsilon_r. \tag{4}$$

Then, formulas (1)–(3) can be calculated by

$$\begin{aligned} \dot{\varepsilon} &= \frac{-2C_0}{l_0}\varepsilon_r, \\ \dot{\varepsilon} &= \frac{-2C_0}{l_0}\int_0^t \varepsilon_r dt, \\ \sigma &= \frac{AE}{A_0}\varepsilon_t. \end{aligned} \tag{5}$$

In addition, gas explosions can be classified into three typical categories by explosion overpressure level, i.e., slow deflagration, fast deflagration, and detonation [34]. Here, we adopted three different overpressures, e.g., 0.5 MPa, 1 MPa, and 2 MPa, to represent the different pressure levels to simulate low deflagration pressure, fast deflagration pressure, and detonation, respectively. The input pressure of the striker bar was set to be equal to the three overpressures, which can be calculated by the following formulas [35, 36]:

$$F_{\text{input}}(t) = S_B E \varepsilon_i(t), \tag{6}$$

$$\varepsilon_i(t) = \frac{2\Delta U(t)}{\beta U K}, \tag{7}$$

where F_{input} is the pressure applied to the incident bar, MPa; S_B is the cross-sectional area of the bar, m^2; E is the elastic modulus of the bar, 2.1×10^5 MPa; $\Delta U(t)$ is the peak value of the voltage signal before the incident wave propagates to the surface of the coal core, which is obtained by the stress-strain acquisition system, V; U is the bridge pressure, 4 V; β is the gain multiple, 100; and K is the sensitivity coefficient of the strain gauge, 2.08.

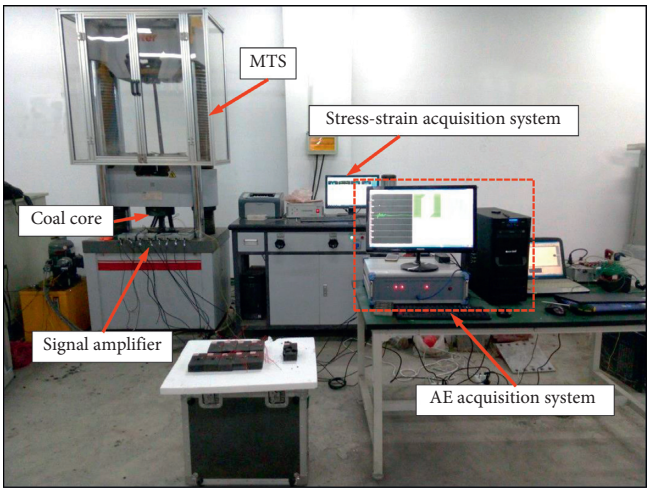

Figure 2: Schematic diagram of the experiment system.

3. Results and Discussion

3.1. Static Mechanical Properties of Coal. The static mechanical parameters of the two kinds of coal cores were measured and shown in Table 2. Each value is the average one from three different tests. As can be seen, the compression strength and Poisson's ratio of the anthracite coal are lower than those of the bituminous coal despite of higher fixed carbon content shown in Table 1.

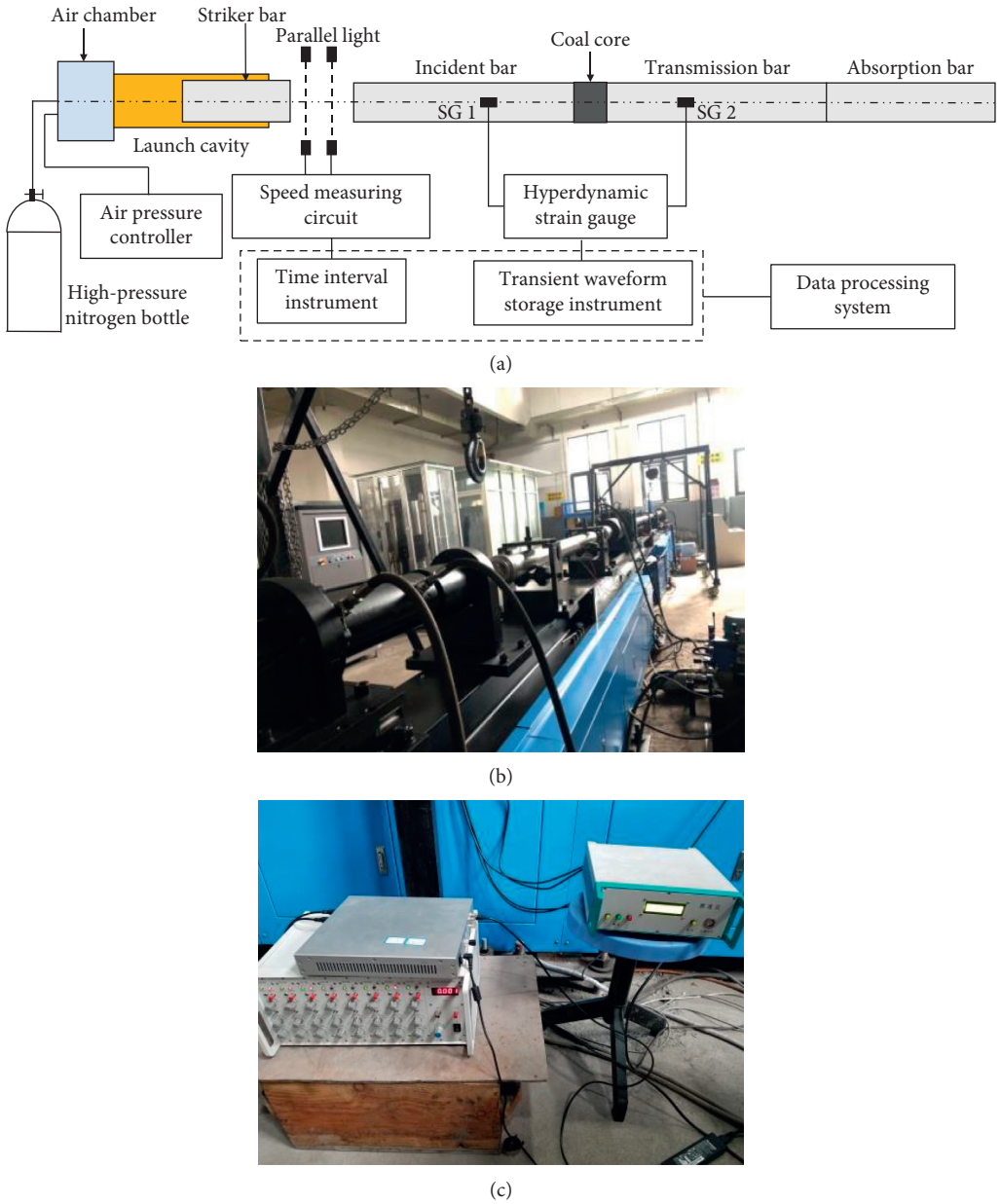

Figure 3: Dynamic mechanical properties test system. (a) Schematic diagram of SHPB, (b) compression bar system, and (c) data acquisition system.

Figure 4 shows that the strain and stress increased as the compression loading was applied and then decreased suddenly. And, the compression failure process of the coal cores can be divided into four stages, which is similar to the findings of Rashed and Peng [37].

(1) Elastic Deformation Stage (OA). The stress and strain increased linearly under the compression loading. However, the loading was still much lower than the coal's compression strength.

(2) Pore Compaction Stage (AB, Linear Strain Hardening). When the compression loading kept increasing, the microcracks and pores in coals were compacted and new cracks had not yet developed, during which the stress maintained at a nearly constant value while the strain increased dramatically. And, the acoustic emission signal is not significant at this stage. Besides, the stress of both the anthracite coal and the bituminous coal increased by 4%. The strain of the anthracite coal increased by 0.36%, while it increased by 0.66% for the bituminous coal. Figure 5 shows that the total pore volume of the anthracite coal is nearly 30 times that of the bituminous coal. However, the strain variation seemed to be not well corresponding to the total pore volume. This indicates that other factors are also crucial in the process.

Table 2: Basic mechanical parameters of coal.

Materials	Compression strength (MPa)	Elastic modulus (GPa)	Poisson ratio
Anthracite coal	8.57	1.01	0.201
Bituminous coal	15.96	0.92	0.32

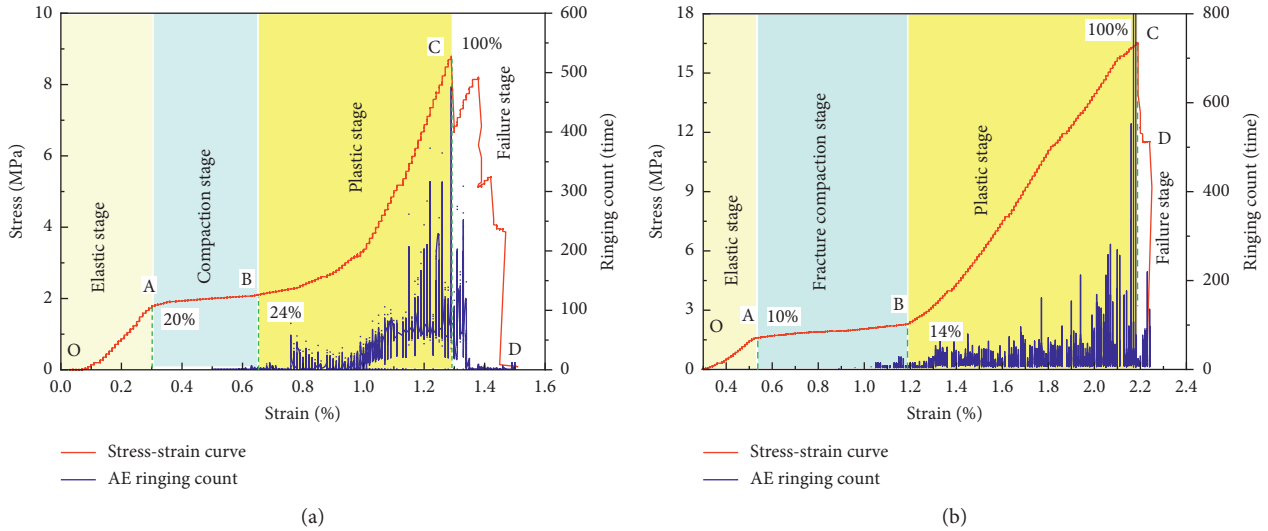

Figure 4: Stress-strain curves and acoustic emissions under uniaxial compression. (a) Anthracite coal and (b) bituminous coal.

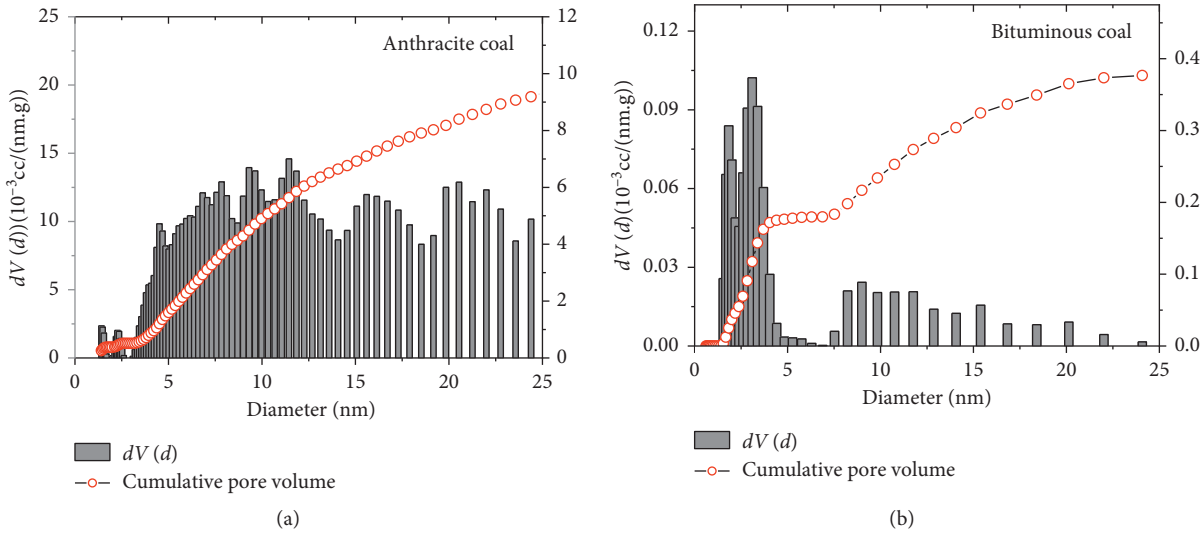

Figure 5: Pore size distributions of coals. (a) Anthracite coal with a total pore volume of 11×10^{-3} cc/g; (b) bituminous coal with a total pore volume of 0.38×10^{-3} cc/g. Pore size distribution was calculated by nonlocal density functional theory (NL-DFT).

(3) Plastic Deformation Stage (BC, Parabolic Strain Hardening). The stress and strain indicated a parabolic relationship until reaching the compression strength. The compression strength of the anthracite coal and the bituminous coal is 8.57 MPa and 15.96 MPa, respectively. Besides, the increase of AE ringing counts also indicated that new cracks in coals began to develop steadily.

(4) Failure Stage (CD). The stress-strain curve of the bituminous coal showed a sudden downtrend. However, the anthracite coal showed a downward trend with oscillations, which indicates that it did not rupture immediately after reaching compression strength. At this stage, cracks developed rapidly in coal cores and the microcracks grew into large macrocracks. Meanwhile, the AE ringing count of the coals dropped rapidly.

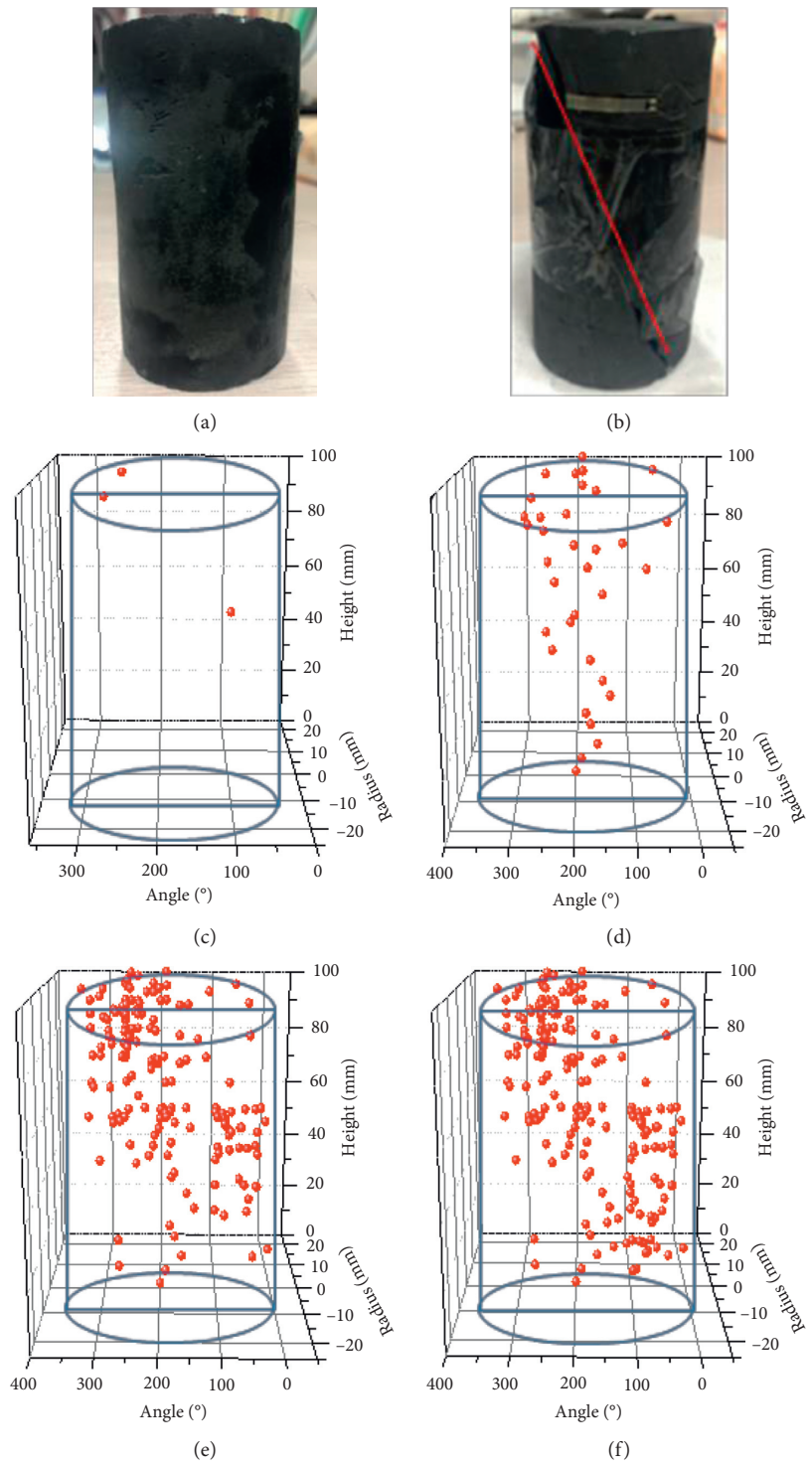

FIGURE 6: Acoustic emission of bituminous coal cores at different stress levels. (a) Original sample; (b) failure sample; (c) 20% σ_c; (d) 40% σ_c; (e) 80% σ_c; and (f) 100% σ_c, where σ_c is the compression strength.

The above results show that both anthracite coal and the bituminous coal indicated brittle failure, respectively, according to the criterion proposed by some former researchers [38, 39].

In addition, when the applied stress on the coals is greater than its mechanical strength, the initial cracks will yield and deform, and then the cracks will expand and release energy in the form of elastic wave, which is the so-called acoustic emission phenomenon [40, 41]. Therefore, tests of the acoustic emission signals releasing from coal cores during uniaxial compression can monitor the whole failure process. The intensity of AE activity and the degree of

Table 3: Experimental results of dynamic mechanics of coals.

Coal core	Pressure in air chamber (MPa)	Striker bar speed ($m \cdot s^{-1}$)	Strain rate (s^{-1})	Compressive strength (MPa)	Ultimate strain	Elasticity modulus (GPa)
A-1	0.05	1.68	273.74	76.0	0.0359	2.71
A-2	0.06	1.99	285.69	122.7	0.0347	16.42
A-3	0.08	2.45	376.90	106.7	0.0461	12.62
B-1	0.05	1.50	217.42	51.6	0.0333	9.27
B-2	0.06	1.97	317.97	89.9	0.0423	9.32
B-3	0.08	2.54	424.05	65.94	0.0601	2.03

damage in rock structures are usually indexed by AE ringing count. The results are given in Figures 4 and 6.

Taking bituminous coal, for example, Figure 6 shows the acoustic emission signals of coal cores under uniaxial compression. It can be seen that the bituminous coal cores followed a shear failure mode, and the evolution process of cracks is as follows:

(1) The microcracks on the left-end face distributed scarcely (20% σ_c)

(2) The cracks on the upper left and middle developed (40% σ_c)

(3) The right- and left-side cracks connected with the lower part of the right (80% σ_c)

(4) The internal cracks run through (100% σ_c) and macroscopic cracks formed as shown in Figure 6(b)

3.2. Response of Coals to Low-Speed Dynamic Loading. Gas explosions can be classified into three categories by pressure level in intensity, i.e., slow deflagration, fast deflagration, and detonation. Therefore, three different pressures were selected to characterize explosive damage, namely, 0.5 MPa, 1 MPa, and 2 MPa. Determining the pressure in air chamber to be 0.05 MPa, 0.06 MPa, and 0.08 MPa. The experimental results of dynamic mechanics of coals are shown in Table 3.

3.2.1. Dynamic Stress-Strain Curves of Coals. Figure 7 gives typical dynamic stress-strain curves of the coal cores (0.06 MPa pressure, for example). Each dynamic stress-strain curve can be divided into four stages:

(1) *Linear Elastic Stage (OA).* The curves show a sharper increase at the initial stage. The modulus of elasticity of the anthracite coal and bituminous coal is 16.42 GPa and 9.32 GPa, respectively, which is much higher than that obtained in the static mechanical properties test which indicates that coals had stronger deformation resistance under dynamic loading.

(2) *Nonlinear Stage (AB).* The dynamic compression strength of the coal increased significantly and showed a distinct strain hardening effect due to significant plastic deformation. At this stage, the microcracks in the sample will increase and expand rapidly under the dynamic loading. Some microcracks converged with each other and broke through to form the main cracks. Macroscopic failure occurred at point B with the development of main cracks.

(3) *Unloading Stage (BC).* The ultimate strain at point C of the anthracite coal was lower than that of the bituminous coal, but its peak stress at point B was higher, which indicates that the anthracite coal has higher dynamic compression strength and lower deformation resistance than the bituminous coal. At this stage, there were a large number of macroscopic fractures in the coal, and the coal deformed rapidly.

(4) *Curve Rebound Segment (CD).* The strain at this stage showed an obvious hysteretic phenomenon, which indicated that the coal core still had partial compression resistance. When the dynamic loading stress was lower than the elastic force stored inside the coal core in the unloading stage, the coal core deformation would rebound greatly, which resulted in the total strain decreases. Besides, when the coal was completely broken, the rebound stopped.

Figure 8 shows the dynamic stress-strain curves of the anthracite coal and the bituminous coal under different dynamic loading. The dynamic modulus of elasticity of the anthracite coal is the largest under 0.06 MPa at the initial stage and followed by 0.08 MPa and 0.05 MPa, which indicates that the anthracite coal has the strongest deformation resistance at 0.06 MPa. The dynamic modulus of elasticity of the bituminous coal at 0.05 MPa and 0.06 MPa is very close, which is higher than that at 0.08 MPa. The ultimate stress is usually defined as dynamic compression strength. The dynamic compression strength of coal cores is the largest at 0.06 MPa. The dynamic compression strength is obviously larger than static compression strength as found by former researchers [42]. The maximum compression strength of the bituminous coal is 5.63 times its maximum static strength, while that of the anthracite coal is 14.32 times its static compression strength.

3.2.2. Dynamic Impact Parameters. Figure 9 summarizes the dynamic mechanical parameters of the coals. As can be seen, the dynamic compression strength and the elasticity modulus are both much higher than those obtained in the static mechanical properties test as shown in Table 2. Meanwhile, the strain rate of the anthracite coal is lower than that of the bituminous coal under a same dynamic loading except the one at 0.05 MPa. The ultimate strain increases with the increase of pressure. Because as the pressure in the air

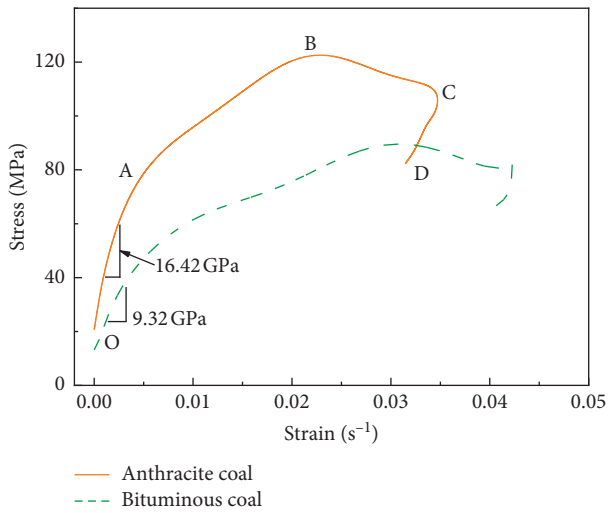

Figure 7: Stress-strain curves of coal cores under dynamic loading (corresponding to pressure in the air chamber = 0.06 MPa).

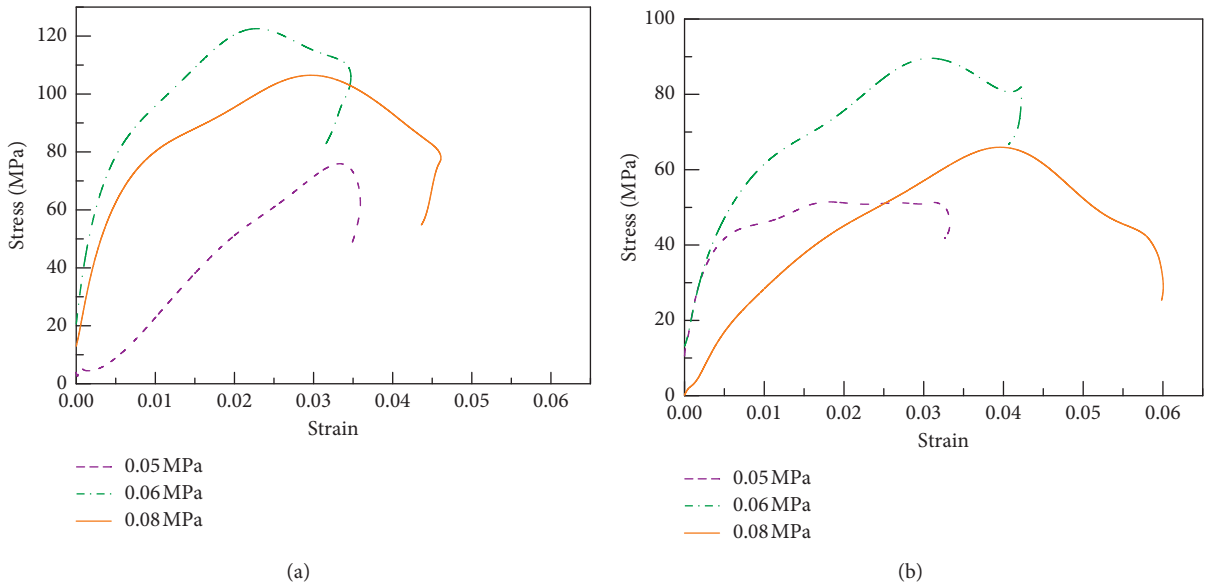

Figure 8: The stress-strain curves of coals under different dynamic loadings. (a) Anthracite coal and (b) bituminous coal.

chamber increases, the impact loading increases and the deformation of coal increases.

Besides, the dynamic compression strength of the anthracite coal is much larger than that of the bituminous coal (except the one of the anthracite coals at 0.05 MPa), which is contrary to the results of the static mechanical properties test in which the static compression strength of the anthracite coal is lower. This may be caused by the differences in coal pore (or fracture) distribution and the physical properties (mainly characterized by the proximate analysis results shown in Table 1). The loading speed of the static mechanical properties test was very slow, and the coal pore (or fracture) distribution might play a more important role. Due to the more abundant pores (or fractures) of the anthracite coal as shown in Figure 5, the static compression strength of the anthracite coal is lower. However, under the dynamic loading, the loading speed was much higher, the impact of the coal pore (or fracture) on the dynamic compression strength was not significant (no obvious pore compaction stage in the stress-strain curve shown in Figures 7 and 8), and the physical properties played a more significant role. Therefore, the anthracite coal tended to have a larger dynamic compression strength due to a higher fixed carbon content.

Ultimate strain is one of the basic mechanical parameters of coal or rock, which can characterize the ultimate deformation of the material. Figure 10 shows the relationship between ultimate strain and strain rate. The ultimate strain

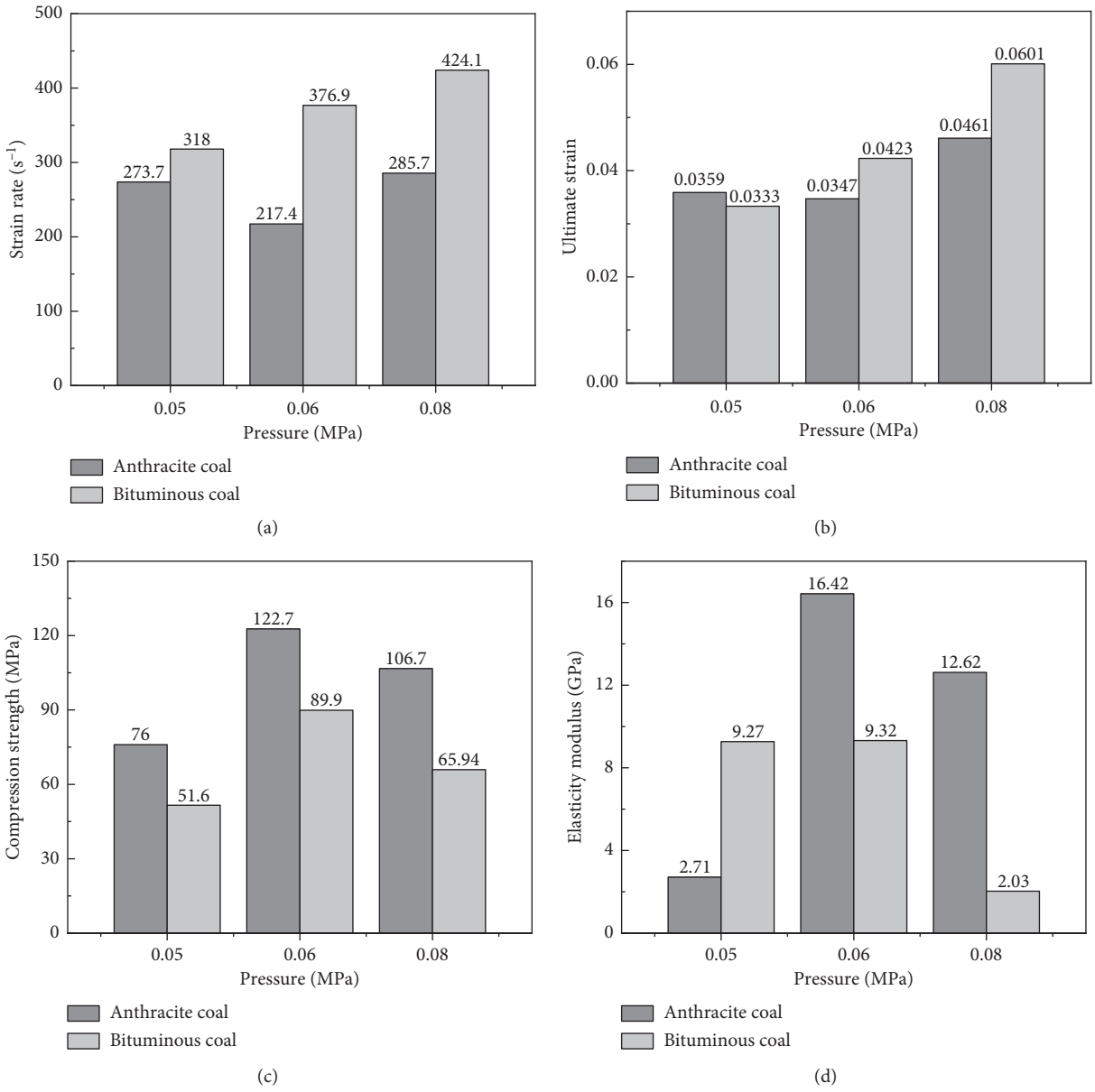

Figure 9: Experimental results of dynamic mechanical parameters of coals. (a) Strain rate, (b) ultimate strain, (c) compression strength, and (d) elasticity modulus.

of the anthracite coal and the bituminous coal both increased linearly with respect to the strain rate, which indicates that the coal with stronger deformation resistance (with lower strain rate) had smaller ultimate strain. Besides, the ultimate strain of the bituminous coal is larger than that of the anthracite coal due to fewer natural cracks shown in Figure 11 and less pores shown in Figure 5.

3.2.3. Absorbed Energy and Its Relationship with the Strain Rate. In the SPHB experiments, the involved energy includes the impact kinetic energy (W_I), the transmitted energy (W_T), and the reflected energy (W_R). Besides, vaseline is applied to both ends of the coal core as a lubricant, so energy loss due to the frictional force between the bar and the coal core is negligible. Thus, the absorbed energy contributing to coal failure can be calculated by

$$W_D = W_I - W_R - W_T. \tag{8}$$

The coal core damage level is related to the energy of the absorbed stress wave, which can be expressed by energy dissipation rate N:

$$N = \frac{W_D}{W_I} \times 100\%. \tag{9}$$

From equations (8) and (9), the calculated results are shown in Figure 12. The total energy increases with the increase of impact pressure as expected, which is due to the

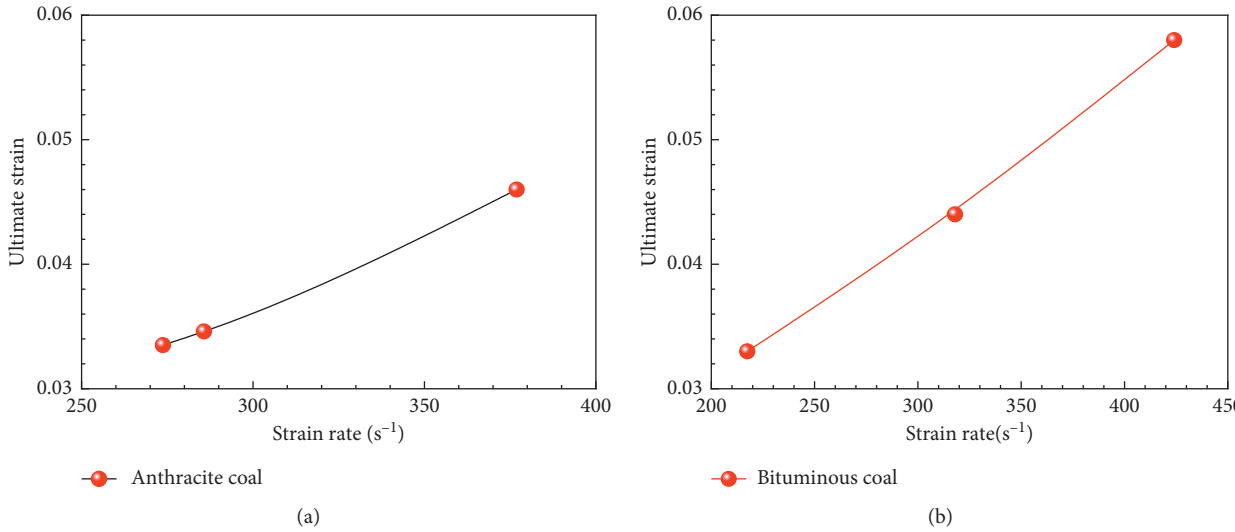

FIGURE 10: The relationship between ultimate strain and strain rate. (a) Anthracite coal and (b) bituminous coal.

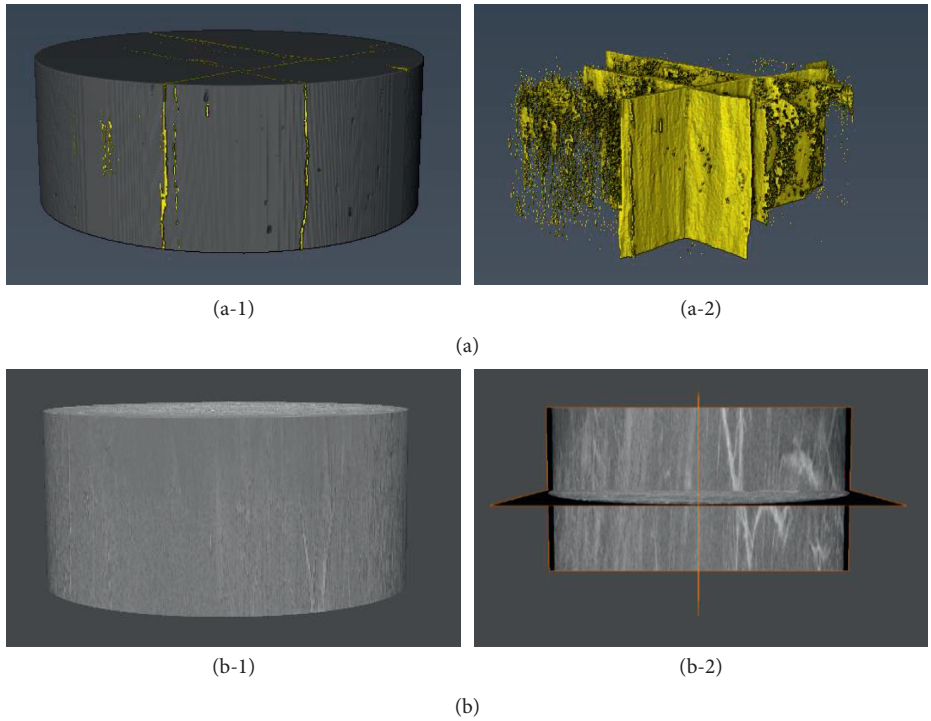

FIGURE 11: CT scan results of natural cracks in coals. The yellow color indicates the cracks. (a) Anthracite coal. (b) Bituminous coal. The subscript "1" represents the scanned coal cores, and the subscript "2" represents the cracks in coal cores.

growth of impact kinetic energy of the striker bar. Meanwhile, the absorbed energy, which directly contributes to the failure of the coal, also increased with the impact loading for both the kinds of coals. In addition, under low impact loading (0.05 MPa), the absorbed energy of the anthracite coal is higher than that of the bituminous coal. However, under high impact loading (0.06.0 MPa and 0.08 MPa), the absorbed energy of the bituminous coal was higher.

The deformation and failure of coal and rock under dynamic loading are closely related to the absorbed energy [43]. The relationship between the strain rate and the absorbed energy is shown in Figure 13. The absorbed energy

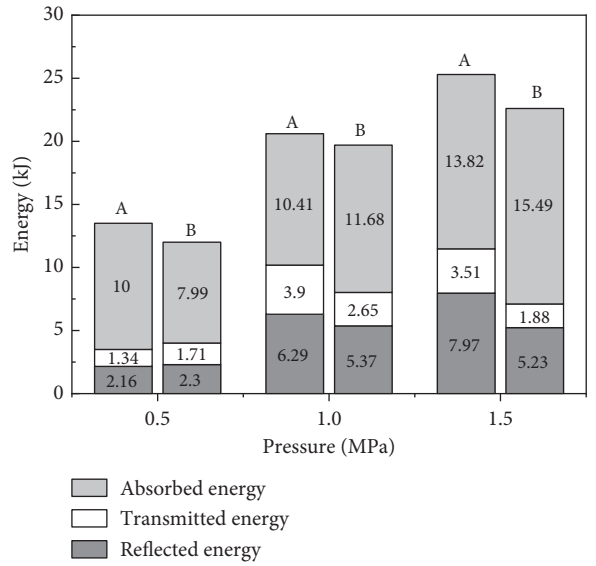

Figure 12: The relationship between energy and dynamic pressure. *A* indicates the anthracite coal and *B* is the bituminous coal.

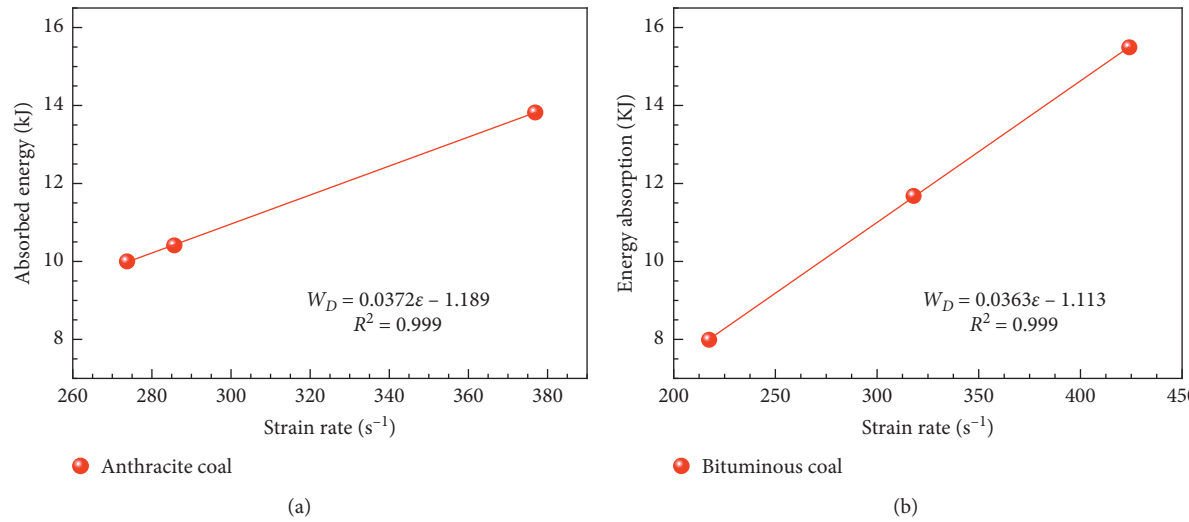

Figure 13: The relationship between strain rate and absorbed energy. (a) Anthracite coal. (b) Bituminous coal. The absorbed energy (W_D) of the two kinds of coal cores is fitted as a function of strain rate by the formula $W_D = a\varepsilon + b$, where a and b are the fitting parameters.

increased linearly with the increase of strain rate, which was also found by Li et al. [44]. Moreover, the difference between the anthracite coal and the bituminous coal is not obvious, which indicates that the absorbed energy is independent of coal type in our experiments.

3.2.4. Fragmentation of Coal under Dynamic Loading. Figures 14 and 15 show the crushed morphology of the anthracite coal and the bituminous coal under different dynamic loading. The statistics of fragment area distribution were conducted, which is counted by the grid method to classify different fragments [45]. As can be seen, with the increase of the dynamic loading, the fragment size of the anthracite coal decreased obviously, while the number of fragments increased. The bituminous coal was split into two halves (i.e., tensile stress failure) at 0.05 MPa. The microcracks in bituminous coal continued to expand with the increase of dynamic loading, and the number of fragments increased.

Meanwhile, the coal will rupture into more small-scale fragments when adsorbing more energy [44]. In our experiments, the coal cores absorbed more energy at high dynamic loading, and there were more small-scale fragments, especially the fragment size in the range of 0–10 cm^2. Similar observations have also been found by Grady and Kipp [46, 47]. Under this low-speed dynamic loading, the mechanical response of the coal is quite different, the degree

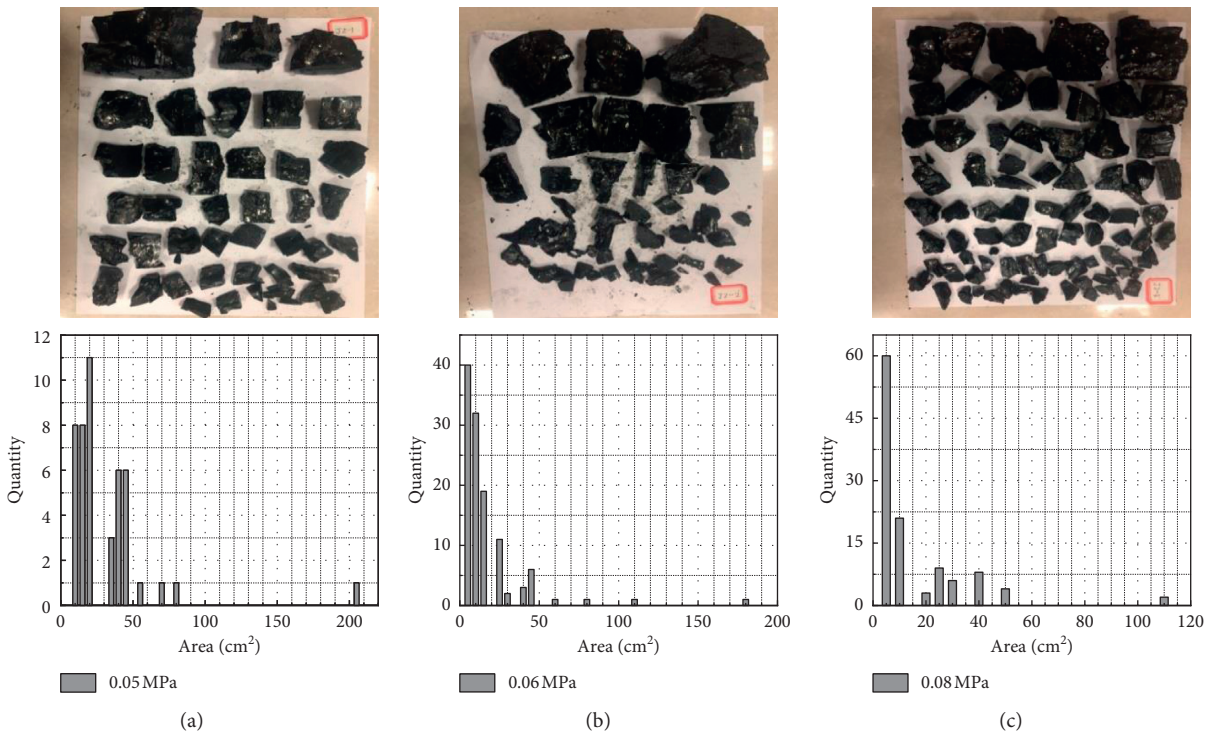

Figure 14: The crushed anthracite coal under different dynamic loading. (a) 0.05 MPa, (b) 0.06 MPa, and (c) 0.08 MPa. The photos above are crushed coal cores, and the bar charts below show their corresponding fragment size distribution.

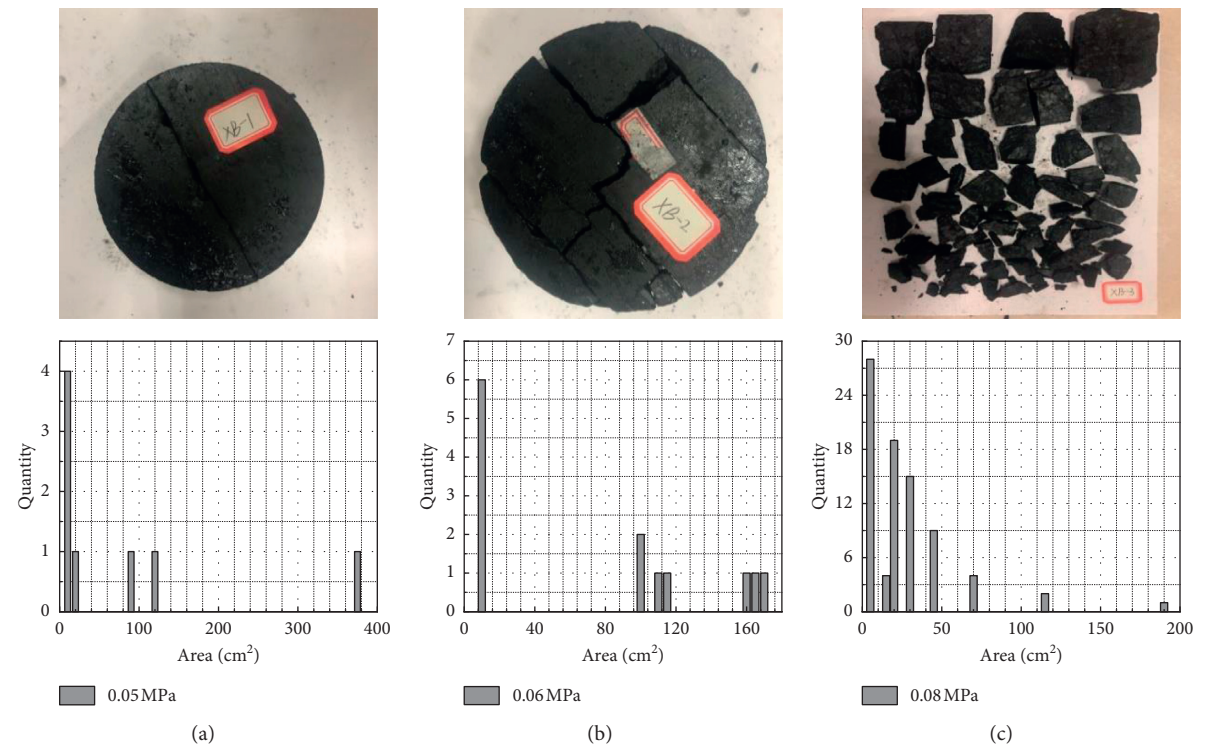

Figure 15: The crushed bituminous coal under different dynamic loading. (a) 0.05 MPa, (b) 0.06 MPa, and (c) 0.08 MPa. The photos above are crushed coal cores, and the bar charts below show their corresponding fragment size distribution.

of failure is smaller (bigger distinguishable fragments), and energy absorbed is less than traditional dynamic loading (unformed powders and smaller fragments). Besides, the anthracite coal had more small-scale fragments comparing to the bituminous coal under a same dynamic loading, which is mainly due to more natural cracks of the anthracite coal shown in Figure 11.

4. Conclusions

(1) In the static mechanical properties test, both coal cores have undergone elastic deformation stage, pore compaction stage, plastic deformation stage, and failure stage. Among them, the anthracite coal and bituminous coal belong to brittle failure.

(2) The dynamic compression strength and elastic modulus are much larger than the static ones. The dynamic strain shows obvious hysteresis phenomenon in the curve rebound stage. The ultimate strain and absorbed energy increased linearly with the increase of strain rate. And, the ultimate strain of the bituminous coal is larger than that of the anthracite coal.

(3) With the increase of dynamic loading, the fragment size of coal cores decreased obviously, while the number of fragments rose, showing a significant strain rate correlation. The strain rate effect of anthracite coal is more sensitive than bituminous coal, and the damage degree is higher.

Data Availability

The data used to support the findings of this study are included within the article.

Conflicts of Interest

The authors declare that they have no conflicts of interest.

Acknowledgments

Financial support provided by the National Natural Science Foundation of China (NSFC) (Grant no: 51874293), National Science and Technology Major Project (Grant No. 2018YFC0807905), Nature Science Foundation of China (51704111 and 51374003), and Scientific Research Fund of Hunan Provincial Education Department (18A187) for this research is gratefully acknowledged.

References

[1] Y. Chunli, L. Xiangchun, R. Yanbin, Z. Yiliang, and Z. Feifei, "Statistical analysis and countermeasures of gas explosion accident in coal mines," *Procedia Engineering*, vol. 84, pp. 166–171, 2014.

[2] F. G. Li and L. Chen, "Gas explosion effect on structure damage and control measures," *Applied Mechanics and Materials*, vol. 501–504, pp. 2424–2427, 2014.

[3] Y. Fu, P. Mao, Y. Mao, and S. Zhang, "Prevention of mine gas disasters in coal mine," in *Proceedings of the International Conference on Automation*, Ji'nan, China, April 2015.

[4] R. K. Zipf, M. J. Sapko, and J. F. Brune, *Explosion Pressure Design Criteria for New Seals in U.S. Coal Mines*, pp. 1–76, Office of Mine Safety and Health Research, National Institute for Occupational Safety and Health (NIOSH), Washington, DC, USA, 2007.

[5] Q. Meng, M. Zhang, L. Han, H. Pu, and T. Nie, "Effects of acoustic emission and energy evolution of rock specimens under the uniaxial cyclic loading and unloading compression," *Rock Mechanics and Rock Engineering*, vol. 49, no. 10, pp. 3873–3886, 2016.

[6] W. Lu, J. Yang, P. Yan et al., "Dynamic response of rock mass induced by the transient release of in-situ stress," *International Journal of Rock Mechanics and Mining Sciences*, vol. 53, pp. 129–141, 2012.

[7] S. T. Yaméogo, R. Corthésy, and M. H. Leite, "Influence of rock failure and damage on in situ stress measurements in brittle rock," *International Journal of Rock Mechanics and Mining Sciences*, vol. 61, pp. 118–129, 2013.

[8] J. C. Li, G. W. Ma, and Y. X. Zhou, "Analytical study of underground explosion-induced ground Motion," *Rock Mechanics and Rock Engineering*, vol. 45, no. 6, pp. 1037–1046, 2011.

[9] M. M. Murphy, E. C. Westman, A. Iannacchione, and T. M. Barczak, "Relationship between radiated seismic energy and explosive pressure for controlled methane and coal dust explosions in an underground mine," *Tunnelling and Underground Space Technology*, vol. 28, pp. 278–286, 2012.

[10] M. Tao, A. Ma, W. Cao, X. Li, and F. Gong, "Dynamic response of pre-stressed rock with a circular cavity subject to transient loading," *International Journal of Rock Mechanics and Mining Sciences*, vol. 99, pp. 1–8, 2017.

[11] G. Liu, M. Cai, and M. Huang, "Mechanical properties of brittle rock governed by micro-geometric heterogeneity," *Computers and Geotechnics*, vol. 104, pp. 358–372, 2018.

[12] H. Y. Liu, M. Roquete, S. Q. Kou, and P.-A. Lindqvist, "Characterization of rock heterogeneity and numerical verification," *Engineering Geology*, vol. 72, no. 1-2, pp. 89–119, 2004.

[13] S. Y. Wang, S. W. Sloan, H. Y. Liu, and C. A. Tang, "Numerical simulation of the rock fragmentation process induced by two drill bits subjected to static and dynamic (impact) loading," *Rock Mechanics and Rock Engineering*, vol. 44, no. 3, pp. 317–332, 2011.

[14] Y. Jin, J. Yuan, M. Chen, K. P. Chen, Y. Lu, and H. Wang, "Determination of rock fracture toughness K IIC and its relationship with tensile strength," *Rock Mechanics and Rock Engineering*, vol. 44, no. 5, pp. 621–627, 2011.

[15] T. Wang, W. Hu, D. Elsworth et al., "The effect of natural fractures on hydraulic fracturing propagation in coal seams," *Journal of Petroleum Science and Engineering*, vol. 150, pp. 180–190, 2017.

[16] W. Yu-Liang, C. Jie, and Z. Sen-Mao, "The acoustic emission technique research on dynamic damage characteristics of the coal rock," *Procedia Engineering*, vol. 26, pp. 1076–1082, 2011.

[17] K. Liu, Q. B. Zhang, G. Wu, J. C. Li, and J. Zhao, "Dynamic mechanical and fracture behaviour of sandstone under multiaxial loads using a triaxial Hopkinson bar," *Rock Mechanics and Rock Engineering*, vol. 52, no. 7, pp. 2175–2195, 2019.

[18] F. Dai, S. Huang, K. Xia, and Z. Tan, "Some fundamental issues in dynamic compression and tension tests of rocks

using split Hopkinson pressure bar," *Rock Mechanics and Rock Engineering*, vol. 43, no. 6, pp. 657–666, 2010.

[19] J. E. Field, S. M. Walley, W. G. Proud, H. T. Goldrein, and C. R. Siviour, "Review of experimental techniques for high rate deformation and shock studies," *International Journal of Impact Engineering*, vol. 30, no. 7, pp. 725–775, 2004.

[20] B. A. Gama, S. L. Lopatnikov, and J. W. Gillespie, "Hopkinson bar experimental technique: a critical review," *Applied Mechanics Reviews*, vol. 57, no. 4, p. 223, 2004.

[21] X. B. Li, T. S. Lok, J. Zhao, and P. J. Zhao, "Oscillation elimination in the Hopkinson bar apparatus and resultant complete dynamic stress-strain curves for rocks," *International Journal of Rock Mechanics and Mining Sciences*, vol. 37, no. 7, pp. 1055–1060, 2000.

[22] M. N. Bagde and V. Petroš, "Fatigue properties of intact sandstone samples subjected to dynamic uniaxial cyclical loading," *International Journal of Rock Mechanics and Mining Sciences*, vol. 42, no. 2, pp. 237–250, 2005.

[23] S. H. Cho, Y. Ogata, and K. Kaneko, "Strain-rate dependency of the dynamic tensile strength of rock," *International Journal of Rock Mechanics and Mining Sciences*, vol. 40, no. 5, pp. 763–777, 2003.

[24] N. Erarslan and D. J. Williams, "The damage mechanism of rock fatigue and its relationship to the fracture toughness of rocks," *International Journal of Rock Mechanics and Mining Sciences*, vol. 56, pp. 15–26, 2012.

[25] L. Jing, "A review of techniques, advances and outstanding issues in numerical modelling for rock mechanics and rock engineering," *International Journal of Rock Mechanics and Mining Sciences*, vol. 40, no. 3, pp. 283–353, 2003.

[26] X. Li, Z. Zhou, T.-S. Lok, L. Hong, and T. Yin, "Innovative testing technique of rock subjected to coupled static and dynamic loads," *International Journal of Rock Mechanics and Mining Sciences*, vol. 45, no. 5, pp. 739–748, 2008.

[27] Y. Li, J. Peng, F. Zhang, and Z. Qiu, "Cracking behavior and mechanism of sandstone containing a pre-cut hole under combined static and dynamic loading," *Engineering Geology*, vol. 213, pp. 64–73, 2016.

[28] O. Yilmaz and T. Unlu, "Three dimensional numerical rock damage analysis under blasting load," *Tunnelling and Underground Space Technology*, vol. 38, pp. 266–278, 2013.

[29] F. Zhang, J. Peng, Z. Qiu, Q. Chen, Y. Li, and J. Liu, "Rock-like brittle material fragmentation under coupled static stress and spherical charge explosion," *Engineering Geology*, vol. 220, pp. 266–273, 2017.

[30] J. B. Zhu, Z. Y. Liao, and C. A. Tang, "Numerical SHPB tests of rocks under combined static and dynamic loading conditions with application to dynamic behavior of rocks under in situ stresses," *Rock Mechanics and Rock Engineering*, vol. 49, no. 10, pp. 3935–3946, 2016.

[31] C. Huang and G. Subhash, "Influence of lateral confinement on dynamic damage evolution during uniaxial compressive response of brittle solids," *Journal of the Mechanics and Physics of Solids*, vol. 51, no. 6, pp. 1089–1105, 2003.

[32] D. Li, C. C. Li, and X. Li, "Influence of sample height-to-width ratios on failure mode for rectangular prism samples of hard rock loaded in uniaxial compression," *Rock Mechanics and Rock Engineering*, vol. 44, no. 3, pp. 253–267, 2011.

[33] R. Bishop, "Stress waves in solids," *Nature*, vol. 174, p. 527, 1954.

[34] D. Bjerketvedt, J. R. Bakke, and K. van Wingerden, "Gas explosion handbook," *Journal of Hazardous Materials*, vol. 52, no. 1, pp. 1–150, 1997.

[35] C. Chen-Guang, "Study on nonlinear deformation and damage of rock under impulse loading," *Journal of Civil Engineering*, vol. 8, pp. 447–459, 2016.

[36] Y. E. Ren-Chuan and S. Chao-Ming, "Effects and Solutions of SHPB experimental waveform oscillation," *Science Technology & Engineering*, vol. 14, pp. 1–5, 2014.

[37] G. Rashed and S. S. Peng, "Change of the mode of failure by interface friction and width-to-height ratio of coal specimens," *Journal of Rock Mechanics and Geotechnical Engineering*, vol. 7, no. 3, pp. 256–265, 2015.

[38] M. S. Paterson and T.-F. Wong, "Experimental rock deformation-the brittle field," *Mineralogical Magazine*, vol. 43, pp. 1–335, 1979.

[39] X. P. Zhou, Y. J. Lian, L. N. Y. Wong, and F. Berto, "Understanding the fracture behavior of brittle and ductile multi-flawed rocks by uniaxial loading by digital image correlation," *Engineering Fracture Mechanics*, vol. 199, pp. 438–460, 2018.

[40] H. Alkan, Y. Cinar, and G. Pusch, "Rock salt dilatancy boundary from combined acoustic emission and triaxial compression tests," *International Journal of Rock Mechanics and Mining Sciences*, vol. 44, no. 1, pp. 108–119, 2007.

[41] X. Lei, K. Kusunose, M. V. M. S. Rao, O. Nishizawa, and T. Satoh, "Quasi-static fault growth and cracking in homogeneous brittle rock under triaxial compression using acoustic emission monitoring," *Journal of Geophysical Research: Solid Earth*, vol. 105, no. B3, pp. 6127–6139, 2000.

[42] T. Chakraborty, S. Mishra, J. Loukus, B. Halonen, and B. Bekkala, "Characterization of three Himalayan rocks using a split Hopkinson pressure bar," *International Journal of Rock Mechanics and Mining Sciences*, vol. 85, pp. 112–118, 2016.

[43] H. Xie, L. Li, Y. Ju, R. Peng, and Y. Yang, "Energy analysis for damage and catastrophic failure of rocks," *Science China Technological Sciences*, vol. 54, no. S1, pp. 199–209, 2011.

[44] X. B. Li, T. S. Lok, and J. Zhao, "Dynamic characteristics of granite subjected to intermediate loading rate," *Rock Mechanics and Rock Engineering*, vol. 38, no. 1, pp. 21–39, 2004.

[45] B. Q. Lin, C. J. Zhu, B. Y. Jiang, and Q. Liu, "Multiphase destructive effects of shock wave resulting from coal mine gas explosion," *Journal of China University of Mining & Technology*, vol. 42, pp. 718–724, 2013.

[46] D. E. Grady and M. E. Kipp, "The micromechanics of impact fracture of rock," *International Journal of Rock Mechanics and Mining Sciences & Geomechanics Abstracts*, vol. 16, no. 5, pp. 293–302, 1979.

[47] D. E. Grady and M. E. Kipp, "Continuum modelling of explosive fracture in oil shale," *International Journal of Rock Mechanics and Mining Sciences & Geomechanics Abstracts*, vol. 17, no. 3, pp. 147–157, 1980.